New Experimental and Theoretical Approach to the Heterogeneous Hydrolysis of NO_2: Key Role of Molecular Nitric Acid and Its Complexes†

K. A. Ramazan,‡,§ L. M. Wingen,‡ Y. Miller,|| G. M. Chaban,⊥ R. B. Gerber,‡,|| S. S. Xantheas,# and B. J. Finlayson-Pitts*,‡

Department of Chemistry, University of California, Irvine, California 92697-2025

Received: November 7, 2005; In Final Form: December 31, 2005

Although heterogeneous chemistry on surfaces in the troposphere is known to be important, there are currently only a few techniques available for studying the nature of surface-adsorbed species as well as their chemistry and photochemistry under atmospheric conditions of 1 atm pressure and in the presence of water vapor. We report here a new laboratory approach using a combination of long path Fourier transform infrared spectroscopy (FTIR) and attenuated total reflectance (ATR) FTIR that allows the simultaneous observation and measurement of gases and surface species. Theory is used to identify the surface-adsorbed intermediates and products, and to estimate their relative concentrations. At intermediate relative humidities typical of the tropospheric boundary layer, the nitric acid formed during NO_2 heterogeneous hydrolysis is shown to exist both as nitrate ions from the dissociation of nitric acid formed on the surface and as molecular nitric acid. In both cases, the ions and HNO_3 are complexed to water molecules. Upon pumping, water is selectively removed, shifting the $NO_3^--HNO_3(H_2O)_y$ equilibria toward more dehydrated forms of HNO_3 and ultimately to nitric acid dimers. Irradiation of the nitric acid−water film using 300−400 nm radiation generates gaseous NO, while irradiation at 254 nm generates both NO and HONO, resulting in conversion of surface-adsorbed nitrogen oxides into photochemically active NO_x. These studies suggest that the assumption that deposition or formation of nitric acid provides a permanent removal mechanism from the atmosphere may not be correct. Furthermore, a potential role of surface-adsorbed nitric acid and other species formed during the heterogeneous hydrolysis of NO_2 in the oxidation of organics on surfaces, and in the generation of gas-phase HONO on local to global scales, should be considered.

Introduction

Heterogeneous chemistry is important in both the lower and upper atmosphere.[1] In the stratosphere, for example, reactions occurring on polar stratospheric clouds were shown about two decades ago to play a major role in the rapid destruction of ozone at polar sunrise in the Antarctic. Current understanding of heterogeneous reactions in the troposphere is more limited than that for the upper atmosphere, due in part to the wide range of surfaces available for this chemistry, the thousands of compounds present in air, and the variability in such parameters as water vapor concentration, solar intensity, and meteorological conditions.

Despite these complexities, there is increasing evidence that heterogeneous chemistry is important in the troposphere, and in particular in the boundary layer where increased surface area is available in the form of buildings, roads, soil, vegetation, etc. For example, Diamond and co-workers[2−4] have shown that there is an organic layer on the surfaces of buildings and that the composition of this layer changes with location as the air masses move downwind. A particularly striking example of heterogeneous tropospheric chemistry is the hydrolysis of NO_2 on surfaces, which has been recognized for many decades to generate gas-phase HONO:[5−26]

$$2NO_2 + H_2O \xrightarrow{\text{surface}} HONO + HNO_3 \qquad (1)$$

This reaction has been extensively studied because the HONO generated is a major source of OH not only at dawn, but also when averaged over an entire day.[27−36]

Much less attention has been paid to the nitric acid produced in reaction 1. Because it was not observed in the gas phase, which could be more easily monitored in the early studies, HNO_3 was assumed to remain on the surface. This was supported, for example, by measurements of nitrate ions in water rinses of the chamber walls after reaction.[14] The presence of molecular (undissociated) HNO_3 was subsequently observed experimentally using high surface area silica to follow the adsorbed products by infrared spectroscopy.[37,38] If nitric acid remains on the surface, reaction 1 will contribute to the permanent removal of oxides of nitrogen from the atmosphere. Nitric acid generated in the gas phase is removed by wet and dry deposition, either directly or after conversion to particulate ammonium nitrate.

It is commonly assumed that nitric acid deposited on surfaces containing water will dissociate to H_3O^+ and NO_3^-. However, recent laboratory studies suggest that, under some conditions,

† Part of the special issue "David M. Golden Festschrift".

* To whom correspondence should be addressed. Phone: (949) 824-7670. Fax: (949) 824-3168. E-mail: bjfinlay@uci.edu.

‡ Department of Chemistry, University of California Irvine, Irvine, CA 92697-2025.

§ Current address: KLA-Tencor Corporation, One Technology Drive, Milpitas, CA 95035.

|| Department of Physical Chemistry and the Friz Haber Research Center, The Hebrew University, Jerusalem, Israel 91904.

⊥ NASA Ames Research Center, Mail Stop T27B-1, Moffet Field, CA 94035.

Chemical Sciences Division, Pacific Northwest National Laboratory, 906 Battelle Boulevard, P. O. Box 999, MS K1-83, Richland, WA 99352.

10.1021/jp056426n CCC: $33.50
Published on Web 02/23/2006

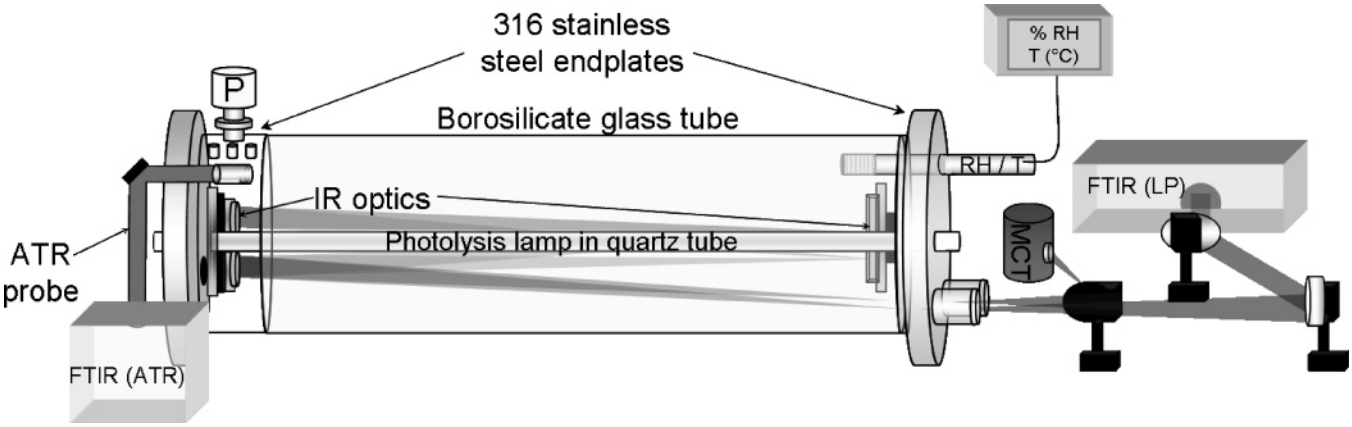

Figure 1. Schematic of the long path−attenuated total reflectance (LP−ATR) apparatus.

the nitric acid adsorbed on the surface is not entirely in the form of nitrate ions, but rather is also in the form of nitric acid−water complexes.[26,39,40] Under some (but not necessarily all)[41] conditions, these complexes can react with NO to generate NO_2, hence recycling the surface-adsorbed nitrate back into photochemically active forms of NO_x.[39,42,43] In addition, photolysis of nitric acid adsorbed on surfaces in the presence of water vapor has been reported to generate gas-phase NO_2, smaller amounts of NO, and HONO.[44−47] This has been hypothesized to be a potentially significant source of daytime HONO. For example, a large midday source of HONO (∼500 ppt h^{-1}) was reported in a recent field study.[48] Finally, there is an "unknown" radical source in large atmospheric smog chambers, which is thought to be at least in part HONO,[49−54] and which may be due to photolysis of surface-adsorbed species such as nitric acid.

The majority of laboratory studies directed at elucidating the kinetics, mechanisms, and products of reaction 1 have focused on monitoring either the gas-phase products (e.g., HONO formation) or, in fewer studies, the adsorbed products. These were typically carried out using high surface area materials to increase the sensitivity for surface species.

We describe here a new apparatus designed to follow simultaneously both the gas-phase and adsorbed reaction products in water films on substrates characteristic of surfaces found in many laboratory systems as well as in the tropospheric boundary layer. This is achieved by coupling in a unique apparatus long path Fourier transform infrared spectroscopy (LP-FTIR) for gas-phase components with an attenuated total reflectance FTIR (ATR-FTIR) probe to follow the chemistry occurring in the surface thin film. Sayer and Horn[55] have described an apparatus that also combines ATR with gas-phase infrared spectroscopic detection, but there are significant differences that are described in more detail below. Our new apparatus is applied to the heterogeneous hydrolysis of NO_2, reaction 1, and theory is used to understand the nature of the surface-adsorbed products. Finally, photolysis of the surface products formed in reaction 1 in two different wavelength ranges is reported. The atmospheric implications are discussed.

We are delighted to contribute this paper in honor of David M. Golden and his 70th birthday, especially since Dave has been a pioneer in laboratory studies of heterogeneous processes in the atmosphere. His development of the Knudsen cell as a tool for studying the uptake of gases on solids and low-volatility liquids set the stage for a large number of studies that followed using this technique. A significant fraction of the heterogeneous atmospheric kinetics known today is based on such Knudsen cell studies. His seminal work on the uptake and reaction of trace gases such as $ClONO_2$ and N_2O_5 with HCl on ice provided key insights into the role of polar stratospheric clouds in Antarctic ozone destruction. And, of course, his contributions to gas-phase kinetics over many decades are legendary. Finally, Dave has shared most generously his time and expertise with the kinetics and atmospheric chemistry communities, including playing a major role in the NASA data evaluations that many of us in these areas consult on an almost daily basis. We look forward to many more years of his contributions and exciting science. Happy Birthday, Dave!

Experimental Section

Combined ATR−Long Path FTIR. Figure 1 is a schematic diagram of the combined ATR−long path FTIR apparatus. The shell of the reaction chamber consists of a cylindrical borosilicate cell that is 30 cm in diameter and 1.2 m in length. Stainless steel endplates on which the optics are mounted increase the total length to 1.4 m, giving a volume of 102 L. A 5.0 cm diameter quartz tube that houses a lamp is located along the center of the reaction chamber, which permits irradiation into the UV beyond the ∼320 nm cutoff for the borosilicate glass from which the outer chamber was constructed. When the surface areas of the cell, quartz tube, endplates, and optics are taken into account, the surface-to-volume ratio is 18.6 m^{-1}. All exposed metal surfaces inside the reaction chamber are covered with halocarbon wax (Halocarbon Products, Inc., Series 1500) to minimize reactivity.

Relative humidity (RH) and temperature (T) are monitored inside the reaction chamber using a Vaisala gauge (HMP-238). Pressures in the range from 10^3 to 0.1 Torr are measured using a Leybold diaphragm gauge (Ceravac CTR-91), and those in the range from 750 to 10^{-4} Torr are measured using a Leybold Pirani Gauge (Thermovac TTR-216). A BOC-Edwards iQDP80/iQMB250 dry pump is used to evacuate the cell while minimizing the backflow of organics associated with oil pumps.

A ThermoNicolet Nexus 670 FTIR spectrometer is used to record infrared spectra of the gas phase. The IR beam is directed from the FTIR via a set of transfer optics into the reaction cell through a ZnSe window. Multiple reflections are achieved using White cell optics,[56] and a total path length of 47.5 m was used in the present studies. The mirrors in the cell were gold coated and protected with a thin layer of SiO. The infrared beam exiting the cell was focused using a 30° off-axis parabolic mirror onto a liquid nitrogen cooled mercury cadmium telluride (MCT) detector.

The ATR probe (Figure 2) is a hollow waveguide probe (Axiom Analytical ATR-FTIR Probe DPR-100) inserted through a vacuum-tight fitting into the reaction chamber. The ATR-

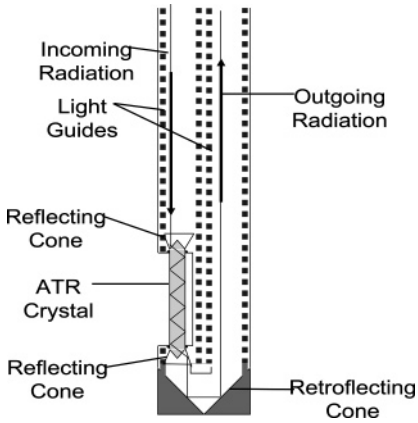

Figure 2. Schematic of the hollow waveguide ATR probe.

FTIR accessory base is placed into the sample compartment of a second FTIR spectrometer (ThermoNicolet Avatar 370). The IR beam in the sample compartment is directed into the infrared transmitting ATR crystal and undergoes total internal reflection. The IR beam reflects nine times within the crystal and is then collected and sent to a cooled MCT detector.

Two infrared crystals were used during these experiments: AMTIR ($Ge_{33}As_{12}Se_{55}$) and silicon (Si). AMTIR has a high IR throughput and wide spectral range (6000−700 cm^{-1}). The surface of the silicon crystal has a thin layer of SiO_x due to exposure to air; hence there are some −Si−OH terminal groups on the surface. This is similar to the surface of the borosilicate glass that comprises most of the surface in the cell; hence we assume that ATR measurements of the thin films using a Si crystal are representative of the majority of the surface chemistry occurring throughout the cell. However, the silicon crystal does not transmit below ∼1500 cm^{-1} due to the oxidized surface layer. As a result, AMTIR was used in the majority of the studies reported here and the silicon crystal was used primarily to validate the observations made over a wider spectral range. In the spectral region above 1500 cm^{-1}, where measurements could be made using both crystals, similar results were obtained using both crystals.

Irradiation of the cell contents, both gas phase and surfaces, is accomplished using lamps located along the axis of the cell. For the experiments described herein, a low pressure mercury lamp (GE, 30 W, G30T8) or a black lamp (Sylvania, 30 W, F30T8/350BL) is used. The low pressure mercury lamp has the strongest line at 254 nm[57] while the black lamp emits a broad range of light from 300 to 400 nm.

The combined LP−ATR FTIR cell described here differs from that of Sayer and Horn[55] in several important respects. First, the ATR crystal and gas-phase long path FTIR are co-located in the same cell, minimizing potential changes in the composition due to transfer of gases from one chamber to another. Second, the White cell optics are designed to give long path lengths (up to ∼100 m) to obtain improved detection for gaseous species. Third, this system can be used in either the static or flow mode, while that of Sayer and Horn[55] is designed for use as a flow system. Finally, the cell contents can be photolyzed using a variety of lamps in order to study photochemical processes.

Experimental Procedures. In a typical experiment, the reaction chamber was filled with a H_2O/N_2 mixture at relative humidities between 37 and 63% to a total pressure of ∼640 Torr by flowing the N_2 gas through a bubbler containing water and mixing it with dry nitrogen in a 5 L mixing bulb. The relative humidity (RH) was measured in both the chamber and the mixing bulb. This mixture was allowed to come to equilibrium for 30 min, and ATR-FTIR and LP-FTIR background spectra were recorded at 1 cm^{-1} resolution with 108−160 coadded scans for the condensed phase and 1 cm^{-1} resolution and 172 coadded scans for the gas phase. This allowed most of the water present in the following spectra to ratio out in the data analysis. Then NO_2 was flushed into the cell as a mixture in nitrogen and the cell was filled to a total pressure of 1 atm with N_2, giving ∼87−250 ppm NO_2. In earlier studies,[26] no difference was observed in the chemistry when the reactions were carried out in air or N_2, so N_2 was chosen in order to minimize NO oxidation. Reaction times up to ∼20 h at a temperature of 296 ± 1 K were typically used, with spectra continuously recorded. At the end of the reaction, the contents of the cell were evacuated for ∼2 h, during which time the cell pressure dropped to $\sim 10^{-2}-10^{-3}$ Torr. Upon cessation of this pumping, the gas-phase and surface film spectra were recorded either under vacuum or after filling the cell to 1 atm with dry N_2.

For the photolysis experiments, the chamber was filled to 1 atm with N_2, and then irradiated for 4 h with either the low pressure mercury lamp or the black lamp. The temperature inside the chamber increased by a maximum of 3 K during the irradiation.

Gas-phase NO_2, HONO, and NO were quantified by the net absorbance of their peaks at 2917, 1263 or 790, and 1875 cm^{-1}, respectively. (While there is a much stronger absorption band for NO_2 at 1620 cm^{-1}, there is significant interference from water vapor that causes additional uncertainty in quantification using this region.) Detection limits for these gases using these bands are 2 ppm for NO_2 and NO and 0.2 ppm for HONO. Concentrations of NO_2 and NO were determined based on calibrations using mixtures of known concentrations in N_2 in the cell. The HONO concentrations were calculated using the 1263 or 790 cm^{-1} band and applying an effective absorption cross section[58] of $(3.7 \pm 0.4) \times 10^{-19}$ cm^2 $molecule^{-1}$ (base 10) or $(2.8 \pm 0.6) \times 10^{-19}$ cm^2 $molecule^{-1}$ (base 10) to measure total HONO based on a trans/cis ratio of 2.3.

Chemicals. Nitric oxide (Matheson, 99%) was purified by passing it through a liquid nitrogen trap to remove impurities such as NO_2 and HNO_3. Nitrogen dioxide was synthesized by reacting the purified NO with excess oxygen (Oxygen Service Company, 99.993%) for at least 2 h. The NO_2 was then condensed in a coldfinger at 195 K and the excess O_2 pumped off. The nitrogen (Oxygen Service Company, 99.999%), air (Oxygen Service Company, <0.1 ppm total hydrocarbons, <0.5 ppm CO, <2.0 ppm H_2O, <0.5 ppm CO_2), and deuterated water (D_2O) (Cambridge Isotope Labs, 99.8%) were used as received. Cyclohexane (Fisher, 99.9%) and cyclohexanone (Aldrich, 99.8%) were placed in a small glass bulb and underwent three freeze−pump−thaw cycles to remove any air and any other low vapor pressure materials in the bulb. The water was Nanopure ASTM type I reagent grade water (Barnstead, 18.2 MΩ cm).

Theory. To guide the interpretation of the experimentally obtained spectra, first principles electronic structure calculations of the magnitude of the shifts in the nitric acid vibrational bands and their theoretical intensities upon complexation with water were carried out. Both harmonic analysis and anharmonic corrections of the fundamentals were carried out for the clusters as described elsewhere.[59,60] The harmonic analysis was performed at the second-order perturbation level of theory (MP2) using the aug-cc-pVDZ basis set.[61,62]

The anharmonic vibrational spectroscopy calculations were carried out by the correlation-corrected vibrational self-consistent field (CC-VSCF) method.[63−65] This method treats both the intrinsic anharmonicity of each mode and the effects due to anharmonic coupling between different normal modes. The CC-VSCF approximation can be used directly with potential points generated from ab initio calculations. In this work, MP2 with a TZP basis set was used for all cases. The CC-VSCF algorithm implemented in the GAMESS package of codes[66] was employed. In this variant, only anharmonic couplings between pairs of normal modes are included, while interactions involving triplets of normal modes or higher order couplings are neglected. Evidence from previous calculations shows that CC-VSCF, including the pairwise mode−mode coupling approximation, is usually of very good accuracy.[65] Part of the results for HNO_3, HNO_3−H_2O, and HONO were published previously.[60] We note that, for the systems studied here, both the intrinsic anharmonicity of individual modes (e.g., OH stretching modes) and the anharmonic coupling between different modes proved significant in cases, depending on the transition. While the effects of anharmonicity on the absolute vibrational frequencies can be substantial, the effect is often much smaller when *frequency shifts* (e.g., between NO_3^- and NO_3^-−H_2O) are considered. Thus, the anharmonic calculations here were restricted to molecular species and to their 1:1 complexes with water. Considerations of frequency shifts were based on the harmonic calculations only. Finally, the intensities of the vibrational transitions were also computed anharmonically, using CC-VSCF.

Results and Discussion

ATR Measurements of Thin Water Films. Attenuated total reflectance (ATR) has been widely used for studying thin films on surfaces.[67] In the present studies, it is assumed that the thin film on the ATR probe is representative of that on the cell walls, so that it monitors the heterogeneous chemistry occurring on the cell surfaces in real time. The film is formed by the uptake of water from the gas phase onto the cell walls and ATR crystal surface, providing the medium for heterogeneous chemistry.

Upon internal reflection of the infrared beam at the surface of the crystal, the evanescent wave penetrates the interface and probes material in contact with the surface. The penetration depth (d_p) of the beam is given by eq I:[67]

$$d_p = \frac{\lambda}{n_1 2\pi(\sin^2\theta - {n_{21}}^2)^{1/2}} \qquad \text{(I)}$$

where λ is the wavelength of the light, n_1 is the refractive index of the denser medium (3.4 for the Si ATR crystal and 2.6 for the AMTIR crystal), θ is the incident angle, and n_{21} is the ratio of the refractive index of the rarer medium (n_2) to that of the crystal (n_1). For bulk water in contact with the AMTIR crystal, for example, the depth of penetration at 3400 cm^{-1} is 0.37 μm. However, as shown below, the average thickness of the water film on this crystal at 50% RH is less than 1 nm. This is sufficiently thin that the evanescent wave penetrates the entire film. In this case, the refractive indices of the ATR crystal and of the media above the film control the electric field more than the refractive index of the film itself, so that n_2 is taken as that of air. The depth of penetration into air at 3400 cm^{-1} for the AMTIR crystal is 0.30 μm.

Figure 3 shows the absorption spectra in the 2500−4000 cm^{-1} region for both the AMTIR and silicon crystals as a function of the relative humidity of the gas phase in equilibrium with the crystal. The uptake is similar for these two materials, suggesting that heterogeneous chemistry that is controlled by water will be similar on AMTIR and silicon, and that the use of AMTIR with its wider spectral range is appropriate for following the surface chemistry in these systems. This is also supported by the similarity of the spectra obtained using the two crystals in the region above 1500 cm^{-1} during the heterogeneous hydrolysis of NO_2 (not shown here).

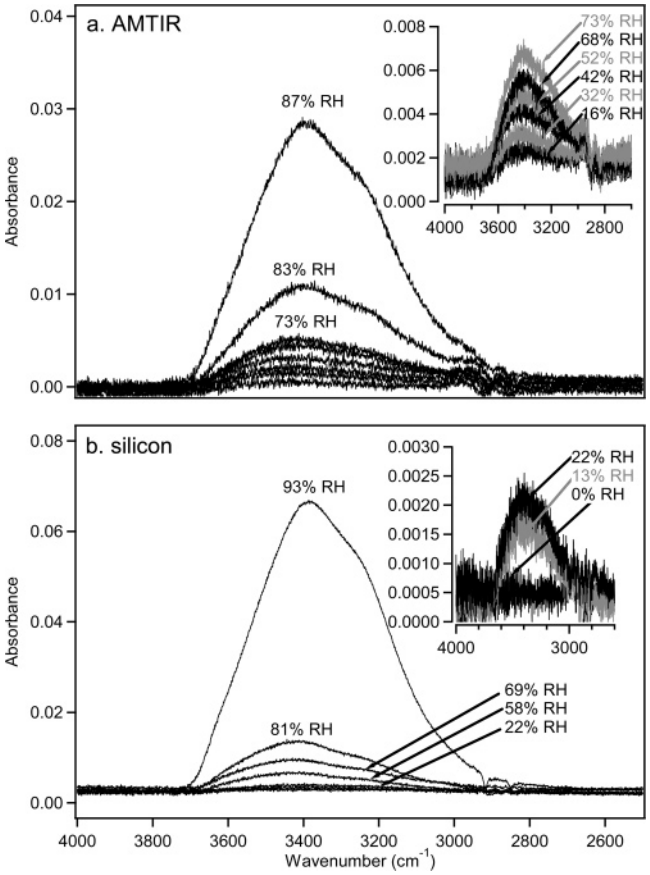

Figure 3. Infrared spectra of water on ATR crystals as a function of relative humidity for (a) AMTIR and (b) silicon at 296 K.

The spectra in Figure 3 at the higher relative humidities are indistinguishable from those of bulk liquid water. Hence the liquid water peak can be used to estimate the effective number of water layers present on the surface as a function of relative humidity. It is not known whether the water is distributed equally over the surface as a smooth film or is in islands. The measurements therefore provide an average, or effective, number of water layers assuming that it is evenly distributed on the crystal. With this caveat, the water coverage, Θ, in number of layers, is calculated from the absorbance spectra using eq II, a modified form of Beer's law:[68]

$$\Theta = \frac{2.303A}{NS_{H_2O}\bar{\sigma}} \qquad \text{(II)}$$

where A is the base 10 integrated absorbance of the liquid water peak from 2800 to 4000 cm^{-1}, N is the number of reflections (nine for this ATR probe), and S_{H_2O} is the surface density of one water monolayer (1.0×10^{15} molecules cm^{-2}). The integrated cross section, $\bar{\sigma}$ (base e), was calculated for the same range to be 1.43×10^{-16} cm $molecule^{-1}$ from optical constants reported by Downing and Williams.[69]

Figure 4 shows the calculated effective number of water layers on the two crystals as a function of relative humidity. AMTIR

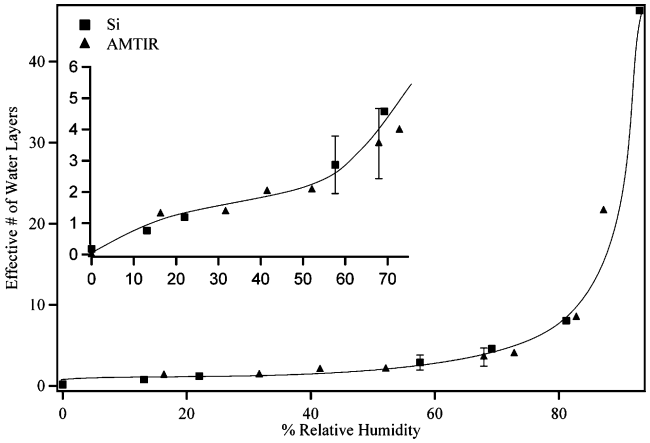

Figure 4. Water uptake isotherms for AMTIR and silicon. Inset is an enlargement of the region between 0 and 75% RH at 296 K.

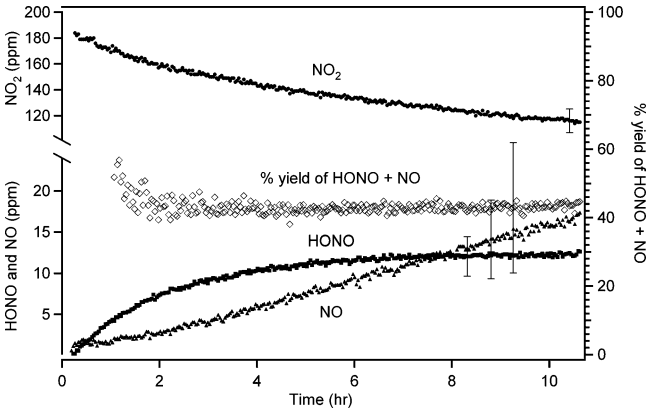

Figure 5. Concentration−time profiles for a typical NO_2 hydrolysis experiment with 184 ppm NO_2 in 1 atm of N_2 at 51% RH. Error bars are $\pm 2s$.

and silicon are similar in their water uptake at relative humidities of 80% and below. At ~50% RH, which was used for most of the experiments reported here, there is the equivalent of ~2 layers of water on the crystal surface, similar to that measured on glass and quartz in earlier studies.[70] It is therefore appropriate to assume that the ATR spectra on both the silicon and AMTIR crystals are representative of the chemistry that is occurring on the cell walls.

Heterogeneous Hydrolysis of NO_2. Since there have been a number of laboratory studies of the heterogeneous hydrolysis of NO_2 (see discussion in the Introduction), we chose this reaction to test our new apparatus. Figure 5 shows a plot of the gas-phase products during a typical experiment at 51% RH. The studies reported here were all carried out at ~50% RH in order to focus on an intermediate water vapor concentration that is typical of atmospheric conditions, but that is also easily generated and controlled under laboratory conditions. As expected, the NO_2 concentration decreases, while both HONO and NO concentrations increase. The sum of the yields of HONO and NO is constant at 44 ± 19% (2*s*), consistent with much of work reviewed in Finlayson-Pitts et al.[26] and within experimental error of 50% expected based on the stoichiometry of reaction 1. We have proposed a mechanism for this reaction previously,[26,47] which is qualitatively consistent with the experimental observations; rate constants for the individual steps are not known at the present time due to the multiple, interdependent processes in the gas phase and on the surface.

Figure 6 shows the ATR spectra of the surface film during the same experiment. The absorption bands at 1316 and 1409

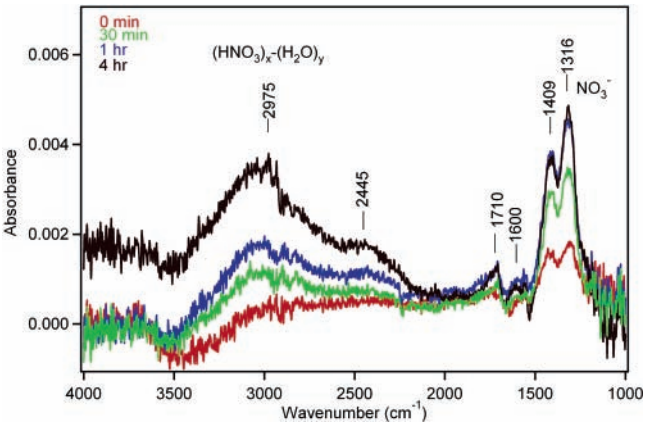

Figure 6. Typical time series of ATR spectra on an AMTIR crystal during the NO_2 hydrolysis experiment shown in Figure 5. $[NO_2]_o$ = 184 ppm and 51% RH.

cm^{-1} are assigned to the well-known ν_3 asymmetric stretch of NO_3^- complexed to water.[59,71,72] The magnitude of the splitting of the degeneracy for this stretch (i.e., the spacing between the peaks) decreases as the amount of water associated with the nitrate ion increases. For example, Ritzhaupt and Devlin[71] observed a splitting of 150 cm^{-1} for HNO_3 in an argon matrix containing 6% water compared to 65 cm^{-1} when the matrix was 100% water. Theory also predicts this trend, with a predicted splitting of 101 cm^{-1} for nitrate associated with four water molecules and 62 cm^{-1} for the complex with five water molecules.[59] The splitting of the peaks in Figure 6 is 93 cm^{-1}, suggesting that about four to five water molecules are associated with the nitrate under these conditions.

The asymmetric NO_2 stretch in nitric acid (monomer or when complexed to water or another HNO_3) is in the 1650−1710 cm^{-1} region[59,71,73−78] regardless of the environment (gas phase, low-temperature matrixes, solid phase). We therefore assign the 1710 cm^{-1} band to nitric acid (without specifying whether it is the monomer or a complex). Following the experiments of Barnes et al.[77] on nitric acid in low-temperature matrixes, we assign the 1600 cm^{-1} band to a nitrogen dioxide−nitric acid complex.

The band at 2975 cm^{-1} (Figure 6) is assigned to molecular nitric acid complexed to water and, as discussed below, to some extent complexed to HNO_3 itself. Support for this assignment comes from comparison to theoretical calculations described in more detail below, as well as from several additional experiments. First, after some time had elapsed to allow the NO_2 hydrolysis to proceed, the cell was pumped out for approximately 2 h. This removed the gas-phase species as well as more volatile species on the surface. Figure 7 compares the ATR spectrum taken at the end of 4 h reaction time to that after pumping. The peak at ~2975 cm^{-1} has blue shifted, by ~200 cm^{-1}, suggesting that this is associated with some species that can be converted to a second compound by removing a more volatile component. Interestingly, the splitting of the peaks in the 1400 cm^{-1} region assigned to NO_3^- does not change significantly, suggesting that water is strongly bound to this ion. However, the shape of the peaks suggests there may be a contribution from an underlying peak upon pumping, which could be due to molecular nitric acid,[73,75] possibly complexed to itself or to water.[59]

Experiments were also carried out in which H_2O was replaced by D_2O. Figure 8 compares the ATR spectrum obtained using D_2O to that using H_2O. The peak at 2975 cm^{-1} for the reaction in H_2O has shifted to ~2275 cm^{-1}, consistent with a deuterium

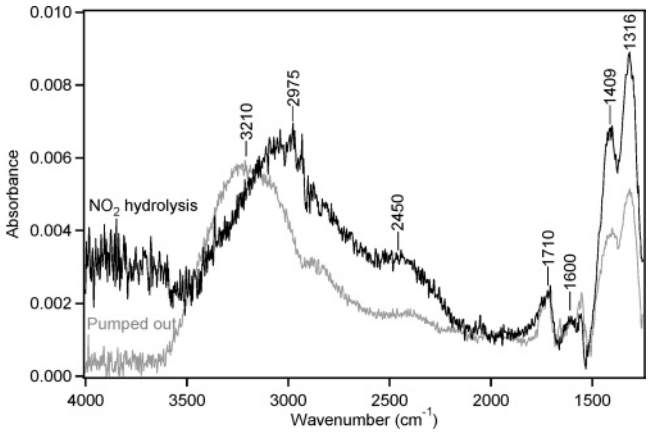

Figure 7. ATR spectra at the end of the NO_2 hydrolysis reaction and after 2 h of pumping. The NO_2 hydrolysis spectrum has been multiplied by 1.82 to normalize it to the pumped-out spectrum in order to match the integrated area of the 1500−1800 cm^{-1} region.

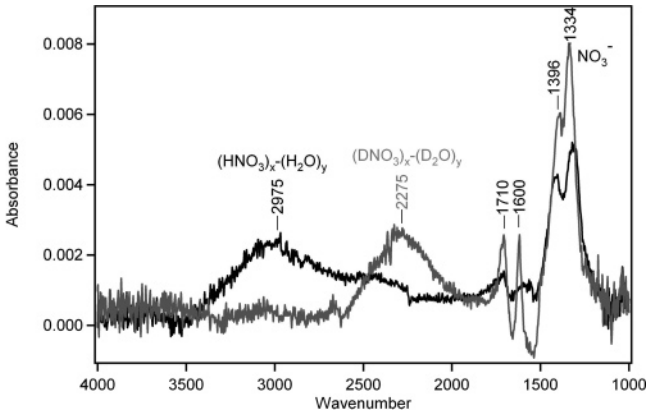

Figure 8. Comparison of ATR spectra from NO_2 hydrolysis using (black spectrum) H_2O and (gray spectrum) D_2O. Water has been ratioed out of both spectra.

isotope effect for an H−O/D−O stretch. The bands in the 1600−1800 cm^{-1} region do not shift, nor do those assigned to NO_3^-, confirming that these are not attributable to vibrations associated with hydrogen.

All of these results are consistent with the peak at 2975 cm^{-1} being due to nitric acid complexed to one or more water molecules. We designate this species as $(HNO_3)_x(H_2O)_y$, where *x* and *y* represent the numbers of nitric acid and water molecules in the surface species. There are several lines of evidence to support this peak assignment. First, theoretical calculations[59,60,78−83] show that complexation of a molecule of nitric acid in the gas phase to one water molecule or to $-SiH_3(OH)$ or $Si(OH)_4$[84] shifts the H−ONO_2 stretch, which occurs at 3550 cm^{-1} in the gas phase, by approximately 500 cm^{-1}. Complexing nitric acid to two or more water molecules further red shifts this vibration.[59,78] Second, the shift from 2975 to 2275 cm^{-1} when D_2O is used in place of H_2O is consistent with a deuterium isotope effect for the H−ONO_2 stretch. Finally, the blue shift of the peak upon pumping suggests that a volatile species, likely water, is being selectively removed from these complexes.

While the 2975 cm^{-1} band is very broad, which is expected for a hydrogen-bonded H−O stretching vibration at room temperature, the shapes of the spectra in Figures 6−8 suggest that this band is comprised of contributions from several species. Deconvolution of the broad peak between 2000 and 3700 cm^{-1} into contributions from four species was accomplished using the following approach. The first contribution was taken to be at 3210 cm^{-1}, based on the blue shift of the peak to this frequency after pumping (Figure 7). This should represent the most dehydrated form of HNO_3 on the surface. On the basis of previous theoretical calculations and experimental studies of HNO_3 in low-temperature inert gas matrixes,[59,71,74,77] this band is assigned to the dimer of nitric acid, $(HNO_3)_2$.

TABLE 1: Summary of Assignment of Infrared Peaks Observed by ATR-FTIR on the Surface in the NO_2 Heterogeneous Hydrolysis at 50% RH at Room Temperature and Comparison to Literature Values

assignment	band position[a] (cm^{-1})	lit. band positions in low-temp matrixes[b] (cm^{-1})
$(HNO_3)_2$	3210	3280 (N_2)[74]
		3216 (Ar)[77]
		3235 (Ar)[59]
$HNO_3{\cdot}H_2O$	2975	3025 (Ar)[59]
$HNO_3{\cdot}2H_2O$	2812	2788 (Ar)[59]
$HNO_3{\cdot}3H_2O$	2450	2600 (Ar)[59]
$HNO_3{\cdot}nH_2O$	1710	1650−1710[59,71,72]
$HNO_3{\cdot}NO_2$	1600	1611 (Ar)[77]
$NO_3^-{\cdot}xH_2O$	1316, 1409	∼1300−1400[59,71,72]

[a] This study. [b] The matrix used is in parentheses.

On the basis of the peak positions in Figures 6−8, the second contribution is taken to be at 2975 cm^{-1}, which we assign to nitric acid bound to one water molecule. This means that complexation of water to the HNO_3 in place of a second HNO_3 (i.e., the dimer) that is responsible for the peak at 3210 cm^{-1} has red shifted the H−ONO_2 stretch by ∼235 cm^{-1}. This is in excellent agreement with the theoretical and low-temperature matrix results of McCurdy et al.,[59] where the shift was observed experimentally to be 210 cm^{-1}, compared to a calculated shift of 181 cm^{-1}.

The third contribution was taken at 2450 cm^{-1} based on the obvious shoulder in this region, and in order to match the experimental data, a fourth peak at 2812 cm^{-1} was also included. These peaks are assigned to $HNO_3(H_2O)_2$ (2812 cm^{-1}) and $HNO_3(H_2O)_3$ (2450 cm^{-1}), respectively. While the existence of the 2812 cm^{-1} peak is not obvious from the spectra, it is consistent with experiments and theoretical calculations for $HNO_3(H_2O)_2$.[59] Furthermore, it would be unusual to have the monohydrate and the trihydrate, but not the dihydrate.

Table 1 compares the peak positions observed here to those from mixtures of HNO_3 with water mostly in low-temperature inert gas matrixes. Given the relatively large width as well as the overlap of the peaks at room temperature in the present studies, and that the surface will impose additional constraints on adsorbed species, the agreement between the band positions observed here and those reported in the literature is very good.

Figure 9 shows the results of deconvoluting an ATR spectrum taken during the NO_2 heterogeneous hydrolysis into four contributing peaks at 3210, 2975, 2812, and 2450 cm^{-1}. There are significant contributions from all four peaks, with that at 2975 cm^{-1} being the largest. Figure 10 shows a similar deconvolution for the spectrum obtained after pumping. The peak at 3210 cm^{-1} is now the most important contributor, and the 2975, 2812, and 2450 cm^{-1} peaks are approximately equal, suggesting that pumping leads to conversion of the higher hydrates of HNO_3 on the surface into the dehydrated, surface-bound dimer of nitric acid.

Changes in the relative intensities of the peaks due to NO_3^- and the nitric acid complexes can be used to obtain some insights into the shifts between the various hydrates and ions on pumping. Table 2 summarizes the peak positions and assignments and the experimentally measured integrated band intensities for these species in a typical experiment. The relative concentrations shown in the last column taking the nitrate ion

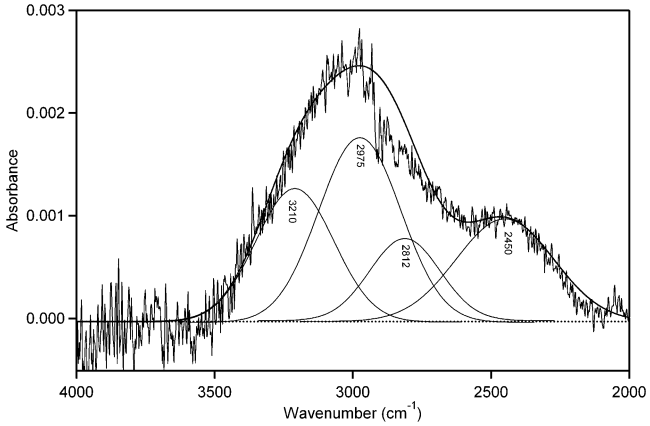

Figure 9. Deconvolution of the ATR absorbance band (Figure 7) between 4000 and 2000 cm^{-1} at the end of NO_2 hydrolysis. The irregular black line represents the spectrum, the dotted black line is the baseline, the smooth black lines are the individual peaks that make up the spectrum, and the solid line through the data is a summation of the individual contributions.

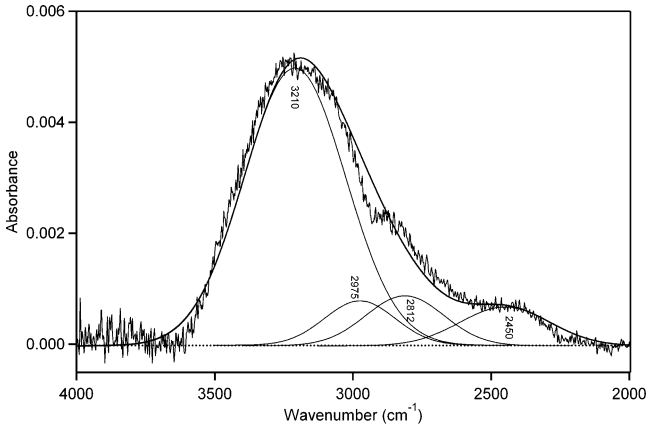

Figure 10. Deconvolution of the broad absorbance (Figure 7) between 4000 and 2000 cm^{-1} after pumping for 2 h. The irregular black line represents the spectrum, the dotted black line is the baseline, the smooth black lines are the individual peaks that make up the spectrum, and the solid line through the data is a summation of the individual contributions.

as the reference, $N_x/N_{NO_3^-}$, were obtained from a Beer−Lambert law type of calculation:

$$\frac{N_x}{N_{NO_3^-}} = \frac{A_x/I_x}{A_{NO_3^-}/I_{NO_3^-}} \qquad \text{(III)}$$

where A_x and $A_{NO_3^-}$ are the experimental integrated band intensities and I_x and $I_{NO_3^-}$ are the calculated theoretical intensities. The theoretical intensity for the nitrate ion was estimated as follows. A value of 845 km mol^{-1} was calculated using the anharmonic approach for NO_3^- complexed to one water molecule. Harmonic calculations predict that the theoretical intensity for $n = 4$ water molecules is 62% of that for $n = 1$, while for $n = 5$ water molecules the theoretical intensity is 78% of that for $n = 1$. Assuming that the 845 km mol^{-1} can be scaled accordingly, and that four to five water molecules are attached to the NO_3^-, an average theoretical intensity for the nitrate complexed to water of 592 km mol^{-1} was derived. Theoretical intensities are available from the harmonic calculations for all of the species identified here, and from the anharmonic calculations for the monohydrate. The theoretical intensity for $HNO_3(H_2O)$ from the anharmonic calculations is 1121 km mol^{-1}, 12% larger than the 999 km mol^{-1} from the harmonic calculations. For consistency, the harmonic values of the theoretical intensities for the higher hydrates and the dimer were therefore adjusted upward by 12%.

TABLE 2: Estimated Concentrations of Nitric Acid Complexes Relative to Nitrate Ions on the Surface during a Typical NO_2 Heterogeneous Hydrolysis Experiment and after Pumping

peak position (cm^{-1})	peak assignment	experimental integrated band intensity (cm^{-1})	ratio of complex concn to nitrate ion concn[a]
	During Hydrolysis		
1316, 1409	$NO_3^-\cdot xH_2O$	0.90	(1.0)[b]
3210	$(HNO_3)_2$	0.46	0.15[c]
2975	$HNO_3\cdot H_2O$	0.66	0.39[d]
2812	$HNO_3\cdot 2H_2O$	0.25	0.10[e]
2450	$HNO_3\cdot 3H_2O$	0.39	0.14[f]
	After Pumping		
1316, 1409	$NO_3^-\cdot nH_2O$	0.625	(1.0)[b,g]
3210	$(HNO_3)_2$	2.3	1.1[c]
2975	$HNO_3\cdot H_2O$	0.25	0.21[d]
2812	$HNO_3\cdot 2H_2O$	0.32	0.18[e]
2450	$HNO_3\cdot 3H_2O$	0.27	0.13[f]

[a] These were obtained from the ratio of (absorbance/theoretical intensity) for each peak to the corresponding ratio for the (1316 + 1409 cm^{-1}) peaks that were assigned to the nitrate ion−water complex. [b] The theoretical intensity for the nitrate ion was estimated as described in the text to be 592 km mol^{-1}. [c] A theoretical intensity of 2043 km mol^{-1} was calculated by adjusting the harmonic value of 1821 km mol^{-1} upward by 12%; this is the amount by which the harmonic and anharmonic calculations differ for the complex of HNO_3 with one water molecule, for which both types of calculations were carried out. [d] A theoretical intensity of 1121 km mol^{-1} from the anharmonic calculations was used for the complex with one water molecule. This is 12% larger than the value of 999 km mol^{-1} from the harmonic model. [e] A theoretical intensity of 1625 km mol^{-1} was used by adjusting the harmonic value of 1448 km mol^{-1} upward by 12%; this is the amount by which the harmonic and anharmonic calculations differ for the complex of HNO_3 with one water molecule, for which both types of calculations were carried out. [f] A theoretical intensity of 1896 km mol^{-1} was used based by adjusting the harmonic value of 1690 km mol^{-1} upward by 12%; this is the amount by which the harmonic and anharmonic calculations differ for the complex of HNO_3 with one water molecule, for which both types of calculations were carried out. [g] On pumping, the nitrate−water peaks decreased to 70% of the intensity at the end of the hydrolysis just prior to pumping. However, for ease of comparison, the relative concentrations of the nitric acid−water complexes are referenced to the nitrate peaks under the same conditions.

There are a number of caveats to be applied to these estimates. First, the calculated theoretical intensities are for gas-phase species, whereas the experimental data are for surface-adsorbed molecules. In addition to the differences that are present for gas versus condensed phase, there is also the possibility of specific interactions with the surface of the crystal in the experiments, for example with surface hydroxyl groups. Second, some of the nitrate may be associated directly with the crystal components rather than only with surface water. Third, there is a possibility of unrecognized complexes contributing to some of the peaks; for example, Thi et al.[85] have reported several different complexes of nitrate ions with nitric acid in thin films. Finally, the amount of material on the crystal, and the corresponding signals, is quite small, so that the estimates of relative concentrations of surface species should be taken as semiquantitative.

However, within these caveats, some conclusions can be drawn from the application of the theoretical assignments of species and band intensities. First, during the NO_2 heterogeneous hydrolysis at 50% RH, the concentrations of the nitric acid−water complexes are significant relative to the nitrate ion,

varying from 10 to 39% of the nitrate ion concentration. In addition, small amounts of HNO_3 dimer are present. On pumping, there is a significant shift in the surface species toward the less hydrated forms of nitric acid, including the nitric acid dimer which becomes the most intense peak (Figure 10). Although nitric acid is a strong acid, it requires association with at least four water molecules[86−88] to dissociate to H^+ and NO_3^- in the gas phase. If pumping removes water preferentially, then dissociation will be impaired and the nitrate ion will be converted first to molecular nitric acid and its complexes with water, and finally to the dimer.

In short, the data are consistent with the formation of both dissociated and undissociated HNO_3 on the surface during the NO_2 heterogeneous hydrolysis, with the nitrate ion and HNO_3 both being complexed to water. Equilibria such as the following are likely involved:

$$HNO_3 + HNO_3 \leftrightarrow (HNO_3)_2 \quad (2)$$

$$HNO_3 + H_2O \leftrightarrow HNO_3 \cdot H_2O \quad (3)$$

$$HNO_3 \cdot H_2O + H_2O \leftrightarrow HNO_3 \cdot 2H_2O \quad (4)$$

$$HNO_3 \cdot 2H_2O + H_2O \leftrightarrow HNO_3 \cdot 3H_2O \quad (5)$$

$$HNO_3 \cdot 3H_2O + xH_2O \leftrightarrow H_3O^+ + NO_3^- \cdot yH_2O \quad (6)$$

When the system is pumped out, the concentrations shift in favor of molecular nitric acid complexed to fewer water molecules and ultimately to the dimer. Thus the extent of ionization on the surface is a sensitive function of the amount of available water. The data in Table 2 can be used to calculate the ratio of the concentration of the nitrate ions using the bands at 1316 and 1409 cm^{-1} to the undissociated nitric acid complexes with water and with a second HNO_3. This gives a ratio of nitrate ions to the complexes of 1.3:1 during the hydrolysis at 50% RH, where there is an effective two layers of water on the surface initially. This suggests that the degree of dissociation of HNO_3 under these conditions is ∼56%. After pumping, the ratio of nitrate ions to the complexes is 0.63:1, corresponding to a degree of dissociation of 39%. This is not surprising, since the degree of dissociation in concentrated bulk aqueous solutions of nitric acid is also small. For example, the degree of dissociation in bulk aqueous solutions varies from 50% at 10 M to only 1% at 22 M.[89] Further evidence for the relatively small extent of ionization of the acid comes from the lack of an underlying broad continuum above 2000 cm^{-1} which is seen in amorphous nitric acid−ice films[75,90] and which has been attributed to proton transfer to form a Zundel-type cation.[91] While quantitative agreement would not be expected between solution-phase data and thin surface films which likely have a more two-dimensional character, the comparison is qualitatively consistent with increased dehydration of the surface film on pumping.

Reaction 6 implies that hydronium ion should be formed in concentrations equal to those of nitrate ions. The bending mode for H_3O^+ in nitric acid trihydrate in ice has been reported[75,76,92] to be in the region around 1750 cm^{-1}. The theoretical intensity for this H_3O^+ band has been calculated[64] to be 139 km mol^{-1}, about a factor of 4 less than that calculated for nitrate complexed to water (592 km mol^{-1}; see footnote *b* to Table 2). A weak shoulder can be seen on the high wavenumber side of the 1710 cm^{-1} peak in Figures 6−8, but its intensity is quite small. This may reflect differences between conditions in the gas phase and those in the surface film, which may affect the width of the band and hence its peak height, as well as the relative theoretical intensities/absorption cross sections.

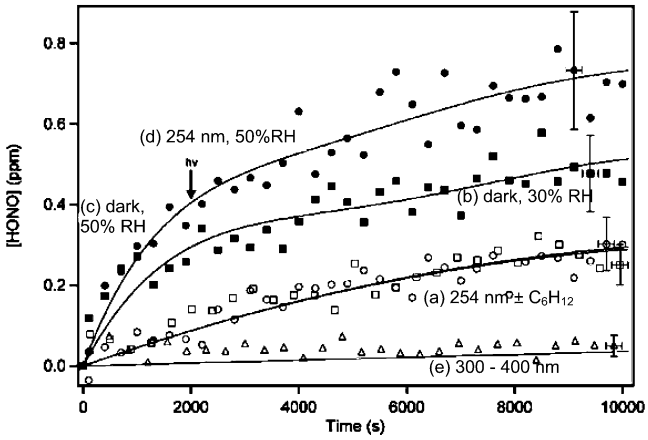

Figure 11. Concentration−time profiles for HONO (a) from irradiation at 254 nm in the absence (○) and presence (□) of an OH scavenger (C_6H_{12}); (b, ■) from exposure to N_2 at 30% RH without irradiation; (c, ●) from exposure to N_2 at 50% RH; (d, △) from exposure to N_2 at 50% RH with irradiation at 254 nm beginning at 2000 s; (e, △) from irradiation using the black lamp (300−400 nm). Each experiment was performed after 20 h of NO_2 hydrolysis followed by pumping for 2 h. All data have been averaged over three data points. Error bars shown in the *x* direction account for the data averaging; error bars in the *y* direction represent the 2*s* experimental and quantification error.

Nitric acid has been observed previously[37,38] as a product on high surface area silica during the heterogeneous hydrolysis of NO_2, based on infrared bands in the 1600−1700 cm^{-1} (asymmetric $-NO_2$ stretch) region. Infrared spectroscopy of silica surfaces treated with pure gaseous nitric acid also suggested that HNO_3 formed surface complexes with water based on absorptions in the H−O stretch region around 3000 cm^{-1}.[26,39,40] The preferential removal of water from these nitric acid treated surfaces by pumping was observed.[26] Sayer and Horn[55] reported that exposure of solid $NaNO_3$ on an ATR crystal to NO_2 gave nitrate and molecular nitric acid, which was attributed to the reaction of NO_2 with small amounts of water on the $NaNO_3$. They observed the loss of a band at 3400 cm^{-1} due to the adsorbed water and an increase in a peak at ∼3000 cm^{-1} which they assigned to H_3O^+. Our studies suggest the latter is due rather to a nitric acid−water complex.

In summary, the studies reported here not only conclusively establish the formation of such complexes during the NO_2 heterogeneous hydrolysis, but also show the progression from ions to increasingly dehydrated forms of nitric acid bound to the surface as water is removed during pumping.

Photolysis of Surface-Adsorbed Species. Given the proposed photolysis of adsorbed nitric acid as a source of HONO in the troposphere,[44,46] a set of experiments was carried out in which the cell surfaces were photolyzed after carrying out the hydrolysis and pumping, followed by filling the chamber to 1 atm with N_2. From the interpretation of the data discussed above, the cell walls should hold adsorbed nitric acid and nitrate under these conditions (Figures 7 and 10). Two lamps were used during separate experiments: (1) a low pressure mercury lamp (primarily 254 nm, with smaller peaks into the UV/visible[57]) and (2) a black lamp (300−400 nm).

Irradiation using the low pressure mercury lamp generated both HONO and NO in the gas phase. Production of NO and HONO from the photolysis of nitric acid in a low-temperature nitrogen matrix was also reported by Chen et al.[93] Figures 11 and 12 show the concentration−time profiles for HONO and NO, respectively, during irradiation. Because both NO and

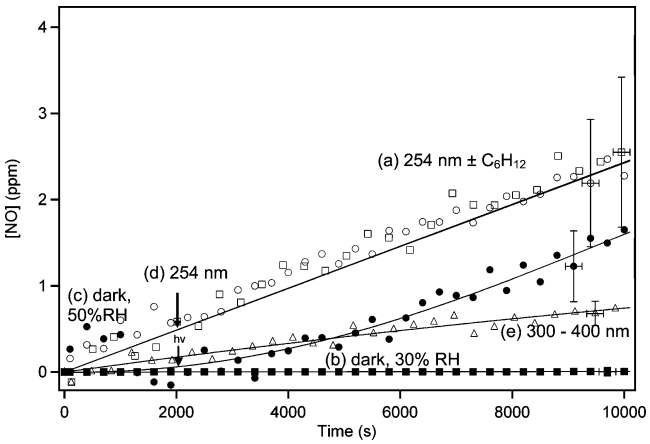

Figure 12. Concentration−time profiles for NO (a) from irradiation at 254 nm in the absence (○) and presence (□) of an OH scavenger (C_6H_{12}); (b, ■) from exposure to N_2 at 30% RH without irradiation; (c, ●) from exposure to N_2 at 50% RH; (d, ●) from exposure to N_2 at 50% RH with irradiation at 254 nm beginning at 2000 s; (e, △) from irradiation using the black lamp (300−400 nm). Each experiment was performed after 20 h of NO_2 hydrolysis followed by pumping for 2 h. All data have been averaged over three data points. Error bars shown in the *x* direction account for the data averaging; error bars in the *y* direction represent the 2*s* experimental and quantification error.

HONO are generated, it is possible that NO is the primary product and that HONO is formed from the recombination of NO with OH radicals. The latter could ostensibly be formed from some process such as nitrate ion photolysis[94] to O^-, which then reacts with residual water to form OH. To test this hypothesis, cyclohexane was added as an OH scavenger in some runs. The reaction between cyclohexane and OH is sufficiently fast ($k = 7.2 \times 10^{-12}$ cm^3 molecule^{-1} s^{-1} at 298 K)[95] that this should have scavenged >95% of any OH that is generated. The open squares in Figures 11 and 12 represent the products in the presence of cyclohexane and the open circles those without cyclohexane; there is no significant impact on the production of HONO (or NO), ruling out the reaction of NO with OH as the source of HONO.

The possibility that NO is generated by HONO photolysis was also considered. The photolysis rate constant for HONO in the cell was measured using a technique described elsewhere,[47] and was found for the low pressure mercury lamp to be $k_p = (1.2 \pm 0.4) \times 10^{-4}$ s^{-1} (2*s*), corresponding to a lifetime of $\tau = 8.3 \times 10^3$ s. This is too slow to produce the NO shown in Figure 12, which increases immediately upon irradiation.

To assess whether increased amounts of water would enhance the HONO and NO production, some runs were carried out in which humidified N_2 was added to the cell after pumping. Previous studies[96] established that borosilicate glass cells that had been exposed to gas-phase HONO and then evacuated became a source of HONO upon exposure to water vapor. Similarly, when water was added to the cell in the present studies after reaction followed by pump down, an increase in gas-phase HONO was also observed (filled squares in Figure 11). When the lamp is turned on during such a run at 50% RH, no enhancement in the HONO production over that due to desorption from the cell walls is observed (filled circles in Figure 11). Similarly, as seen in Figure 12, there is no enhancement in the rate of NO production during irradiation in the presence of water vapor.

When the lamps are turned on, the temperature of the cell rises by a maximum of 3 °C. To test whether HONO and NO could be generated simply by increased thermal desorption, or by desorption of HNO_3 followed by its photolysis to initiate $HO-NO_x$ photochemistry, some experiments were carried out in which the chamber was heated by ~3 °C using heating tape. There was no detectable HONO or NO generated in the gas phase. After 4 h of heating, ~100 ppb gaseous HNO_3 was measured. From a mass balance perspective, desorption of HNO_3 followed by its photolysis is therefore unlikely to be the source of NO and HONO since much larger amounts of NO + HONO, ~3 ppm, are formed in the same time period during irradiation.

Irradiation using the black lamps generated only NO, and at a rate approximately a factor of 4 less than that at 254 nm. The lack of observation of HONO may be due to the smaller light intensities at longer wavelengths and/or to the strong absorption of light in the 300−400 nm region by HONO.[97] The photolysis rate constant for HONO using the black lamps was measured to be $k_p(300-400\ \text{nm}) = (2.0 \pm 0.4) \times 10^{-4}$ s^{-1} (2*s*). Again, the lifetime for HONO photolysis in the cell, $\tau = 5 \times 10^3$ s, is too long to explain the observed NO formation via HONO photolysis. Thus, the difference in photolysis lifetimes using the two lamps is less than a factor of 2 and is unlikely to explain the lack of observation of HONO using the black lamps.

Zhou et al.[46] reported HONO and NO_x (mainly NO_2) production when a glass surface that had been exposed to gaseous HNO_3 and water vapor was photolyzed using a medium pressure mercury lamp with a cutoff filter that only transmitted above 290 nm. In contrast, we observe HONO formation only when 254 nm light is used. However, their sensitivity for HONO is much greater than that using FTIR in the present studies, so that our data do not unequivocally rule out HONO formation during 300−400 nm irradiation. In addition, it is not clear whether the composition of the surface complexes is different when formed from the NO_2 heterogeneous hydrolysis as in our experiments compared to saturating the surface with gas-phase nitric acid and water as in the Zhou et al. experiments.[46]

Thermodynamically, there are a number of potential overall reactions that could generate NO and HONO from the photolysis of surface-adsorbed nitric acid−water complexes. For example, reaction 7

$$HNO_3 + H_2O + h\nu \rightarrow HONO + H_2O_2 \qquad (7)$$

is energetically possible in the gas phase at wavelengths below 741 nm. However, given that there is likely a barrier involved in such a reaction, the actual wavelength of light that would effect such a change is likely significantly shorter. The same applies to reactions 8 and 9 below. Of course, the reaction enthalpy will also be modified by the surface, but this calculation suggests that the low pressure mercury lamps and black lamps both should have sufficient energy to drive such photochemistry. Similarly, reaction 8 is possible at wavelengths below 393 nm:

$$HNO_3\ (+H_2O) + h\nu \rightarrow HONO\ (+H_2O) + O \qquad (8)$$

Generation of NO could occur in a reaction such as

$$HNO_3\ (+H_2O) + h\nu \rightarrow NO\ (+H_2O) + HO_2 \qquad (9)$$

which is energetically accessible at wavelengths below 501 nm, if there is no additional barrier to the dissociation.

Clearly, further work will be required to assess the photochemistry of the surface-adsorbed products of the NO_2 heterogeneous hydrolysis.

Atmospheric Implications. There is increasing evidence that processes occurring on surfaces in the tropospheric boundary layer significantly impact the chemistry and photochemistry in this region. Figure 13 shows the amount of water on the ATR

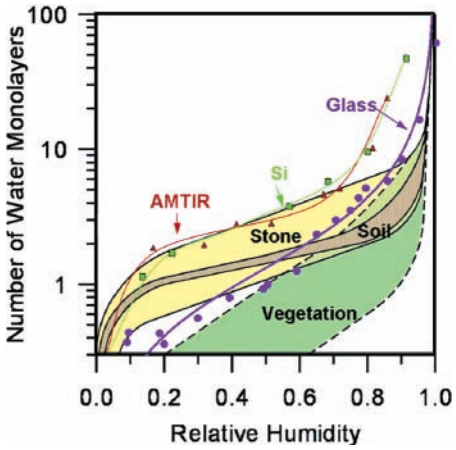

Figure 13. Water uptake on some common atmospheric surfaces (from ref 31) and on AMTIR and silicon ATR crystals.

crystals used here, in comparison to materials present in the boundary layer such as soil and vegetation. Clearly, the amount of water on the surfaces in our experiments is comparable to that on materials found close to the Earth's surface; hence the results reported here should be applicable to chemistry in the boundary layer.

Heterogeneous reactions of oxides of nitrogen, which are precursors to ozone, nitric acid, and airborne particles,[1] are particularly important from local to global scales. Nitric acid is an "end product" of this chemistry, and has been generally assumed to dissociate into nitrate and hydronium ions on surfaces. The work presented here suggests that a significant fraction of nitric acid may exist as complexes with water on atmospheric surfaces such as building materials, foliage, and dust particles, and that photolysis can regenerate gas-phase NO_x ("renoxification"). Thus, formation of nitric acid on surfaces or uptake from the gas phase may not permanently remove NO_x from the atmosphere, as is often assumed.

In addition, oxides of nitrogen, including nitric acid, are associated with significant health effects.[98] Whether the form of nitric acid (i.e., molecular or nitrate ions) plays a role in determining the health impacts of acids and particles is not known, but it is clearly of interest given that much of the acid on the surface of dust particles, for example, will be undissociated molecular HNO_3 complexed to water.

It has been well-documented that there are species of unknown identity on the walls of environmental chambers that generate gas-phase HONO upon irradiation of supposedly "clean" chambers.[49−54] One possibility is that it is the nitric acid−water surface complexes observed here that photolyze to generate HONO. This would be consistent with the experiments of Zhou and co-workers in which HONO production was observed upon photoysis of nitric acid treated glass[46] or of a contaminated sampling system.[44] However, Rohrer et al.[54] reported that HONO generation from the walls of the SAPHIR chamber continued (albeit at a reduced rate) when a filter that only transmitted light above 370 nm was used. The absorption cross sections for gas-phase HNO_3 fall off rapidly above 300 nm,[97] and theoretical studies[99] show that binding of water to nitric acid in the gas phase does not red shift the absorption spectrum significantly. The surface would have to cause very large and unexpected shifts in the electronic absorption spectrum of nitric acid and its water complexes if it were to be the wall source of HONO. However, as discussed above, one of the peaks observed in the ATR spectra is attributed to the nitric acid dimer. Another possibility is the NO_2-HNO_3 complex to which the peak at 1600 cm^{-1} was assigned. Whether the absorption spectrum of the dimer shifts substantially on complexation to a second HNO_3, to NO_2, or possibly to NO_3^- as observed by Thi et al.[85] is not known, but is the subject of ongoing work.

It was observed here as well as in previous studies[96] that gas-phase HONO is generated when a glass surface that had been exposed to gaseous HONO was pumped out and water vapor then added; in contrast, the addition of dry N_2 does not result in gas-phase HONO. Thus either HONO or a HONO precursor must be present on the surface and interact with water to form and/or desorb HONO. This process is very important for the interpretation of HONO concentrations in air and their dependence on RH.[36] Although we did not observe bands in the ATR spectra that were assignable to adsorbed HONO, if it were complexed to nitrate ions or other surface species, the spectra could be shifted significantly compared to that expected based on gas-phase data.

Diamond and co-workers[2−4] have shown that organic compounds are adsorbed on surfaces in the boundary layer, and that the composition of this layer changes from urban to downwind rural sites. Oxidation of organics in air is well-known,[1] and the oxidation products would be expected at least in part to be taken up onto surfaces after formation in the gas phase. The present results raise the possibility that the oxidation may actually occur on the surface itself. In the case of surface films from the NO_2 heterogeneous hydrolysis, the formation of oxygenated and nitrated products could be a marker for such surface oxidations in the boundary layer.

Finally, airborne dust particles are known to become distributed globally,[100−104] impacting global chemistry and climate. Given that dust generally has a high silica content, the chemistry of the oxides of nitrogen described here is expected to occur not only on urban surfaces but also on such dust particles during transport. There is some evidence for HONO production from reactions on dust particles. For example, Stutz and co-workers[35] reported enhanced HONO concentrations during a dust storm in Phoenix, AZ.

These studies are the first to report the simultaneous measurement of both gases and surface species during the heterogeneous hydrolysis of NO_2. While a great deal of insight into the nature of the reaction, its intermediates, and products has been gained, further studies are clearly needed to identify the specific surface species responsible for the production of HONO from surfaces upon exposure to water vapor and upon irradiation.

Acknowledgment. We are especially grateful to Jorg Meyer and Lee Moritz, without whose technical assistance with the design and construction this apparatus would not have been possible. We are also grateful to the California Air Resources Board (Contract No. 00-323) and the National Science Foundation (ATM-0097573, Collaborative Research in Chemistry CHE-0209719 and Environmental Molecular Sciences Institute CHE-0431512) for support of this work. Battelle operates the Pacific Northwest National Laboratory for the Department of Energy. This research was performed in part using the Molecular Science Computing Facility (MSCF) in the William R. Wiley Environmental Molecular Sciences Laboratory, a national scientific user facility sponsored by the Department of Energy's Office of Biological and Environmental Research located at Pacific Northwest National Laboratory.

References and Notes

(1) Finlayson-Pitts, B. J.; Pitts, J. N. *Chemistry of the Upper and Lower Atmosphere: Theory, Experiments and Applications*; Academic Press: San Diego, 2000.

(2) Diamond, M. L.; Gingrich, S. E.; Fertuck, K.; McCarry, B. E.; Stern, G. A.; Billeck, B.; Grift, B.; Brooker, D.; Yager, T. D. *Environ. Sci. Technol.* **2000**, *34*, 2900.
(3) Gingrich, S. E.; Diamond, M. L.; Stern, G. A.; McCarry, B. E. *Environ. Sci. Technol.* **2001**, *35*, 4031.
(4) Lam, B.; Diamond, M. L.; Simpson, A. J.; Makar, P. A.; Truong, J.; Hernandez-Martinez, N. A. *Atmos. Environ.* **2005**, *39*, 6578.
(5) Wayne, L. G.; Yost, D. M. *J. Chem. Phys.* **1951**, *19*, 41.
(6) Cathala, J.; Weinrich, G. *Compt. Rend.* **1952**, *244*, 1502.
(7) Peters, M. S.; Holman, J. L. *Ind. Eng. Chem.* **1955**, *47*, 2536.
(8) Goyer, G. G. *J. Colloid Sci.* **1963**, *18*, 616.
(9) Graham, R. F.; Tyler, B. J. *J. Chem. Soc., Faraday Trans. 1* **1972**, *68*, 683.
(10) England, C.; Corcoran, W. H. *Ind. Eng. Chem. Fundam.* **1974**, *13*, 373.
(11) Ten Brink, H. M.; Bontje, J. A.; Spoelstra, H.; van de Vate, J. F. Atmospheric Pollution 1978. In *Studies in Environmental Science*; Benarie, M. M., Ed.; Elsevier: Amsterdam, 1978; Vol. 1; p 239.
(12) Sakamaki, F.; Hatakeyama, S.; Akimoto, H. *Int. J. Chem. Kinet.* **1983**, *15*, 1013.
(13) Pitts, J. N.; Sanhueza, E.; Atkinson, R.; Carter, W. P. L.; Winer, A. M.; Harris, G. W.; Plum, C. N. *Int. J. Chem. Kinet.* **1984**, *16*, 919.
(14) Svensson, R.; Ljungstrom, E.; Lindqvist, O. *Atmos. Environ.* **1987**, *21*, 1529.
(15) Akimoto, H.; Takagi, H.; Sakamaki, F. *Int. J. Chem. Kinet.* **1987**, *19*, 539.
(16) Jenkin, M. E.; Cox, R. A.; Williams, D. J. *Atmos. Environ.* **1988**, *22*, 487.
(17) Perrino, C.; DeSantis, F.; Febo, A. *Atmos. Environ.* **1988**, *22*, 1925.
(18) Febo, A.; Perrino, C. *Atmos. Environ.* **1991**, *25A*, 1055.
(19) Bambauer, A.; Brantner, B.; Paige, M.; Novakov, T. *Atmos. Environ.* **1994**, *28*, 3225.
(20) Wiesen, P.; Kleffmann, J.; Kurtenbach, R.; Becker, K. H. *Faraday Discuss.* **1995**, *100*, 121.
(21) Kleffmann, J.; Becker, K. H.; Wiesen, P. *Atmos. Environ.* **1998**, *32*, 2721.
(22) Kleffmann, J.; Becker, K. H.; Wiesen, P. *J. Chem. Soc., Faraday Trans.* **1998**, *94*, 3289.
(23) Harrison, R. M.; Collins, G. M. *J. Atmos. Chem.* **1998**, *30*, 397.
(24) Kurtenbach, R.; Becker, K. H.; Gomes, J. A. G.; Kleffmann, J.; Lörzer, J. C.; Spittler, M.; Wiesen, P.; Ackermann, R.; Geyer, A.; Platt, U. *Atmos. Environ.* **2001**, *35*, 3385.
(25) Kotamarthi, V. R.; Gaffney, J. S.; Marley, N. A.; Doskey, P. V. *Atmos. Environ.* **2001**, *35*, 4489.
(26) Finlayson-Pitts, B. J.; Wingen, L. M.; Sumner, A. L.; Syomin, D.; Ramazan, K. A. *Phys. Chem. Chem. Phys.* **2003**, *5*, 223.
(27) Platt, U.; Perner, D.; Harris, G. W.; Winer, A. M.; Pitts, J. N., Jr. *Nature* **1980**, *285*, 312.
(28) Winer, A. M.; Biermann, H. W. *Res. Chem. Intermed.* **1994**, *20*, 423.
(29) Calvert, J. G.; Yarwood, G.; Dunker, A. M. *Res. Chem. Intermed.* **1994**, *20*, 463.
(30) Lammel, G.; Cape, J. N. *Chem. Soc. Rev.* **1996**, *25*, 361.
(31) Lammel, G. *Formation of Nitrous Acid: Parameterization and Comparison with Observations*; Max-Planck-Institut-für Meteorologie: Mainz, 1999.
(32) Alicke, B.; Platt, U.; Stutz, J. *J. Geophys. Res.* **2002**, *107*, DOI: 10.1029/2000JD000075.
(33) Stutz, J.; Alicke, B.; Neftel, A. *J. Geophys. Res.* **2002**, *107*, DOI: 10.1029/2001JD000390.
(34) Alicke, B.; Geyer, A.; Hofzumahaus, A.; Holland, F.; Konrad, S.; Patz, H.; Schafer, J.; Stutz, J.; Volz-Thomas, A.; Platt, U. *J. Geophys. Res* **2003**, *108*, DOI: 10.1029/2001JD000579.
(35) Wang, S. H.; Ackermann, R.; Spicer, C. W.; Fast, J. D.; Schmeling, M.; Stutz, J. *Geophys. Res. Lett.* **2003**, *30*, doi: 10.1029/2003GL017014.
(36) Stutz, J.; Alicke, B.; Ackermann, R.; Geyer, A.; Wang, S. H.; White, A. B.; Williams, E. J.; Spicer, C. W.; Fast, J. D. *J. Geophys. Res.* **2004**, *109*; doi: 10.1029/2003JD004135.
(37) Goodman, A. L.; Underwood, G. M.; Grassian, V. H. *J. Phys. Chem. A* **1999**, *103*, 7217.
(38) Barney, W. S.; Finlayson-Pitts, B. J. *J. Phys. Chem. A* **2000**, *104*, 171.
(39) Rivera-Figueroa, A. M.; Sumner, A. L.; Finlayson-Pitts, B. J. *Environ. Sci. Technol.* **2003**, *37*, 548.
(40) Dubowski, Y.; Sumner, A. L.; Menke, E. J.; Gaspar, D. J.; Newberg, J. T.; Hoffman, R. C.; Penner, R. M.; Hemminger, J. C.; Finlayson-Pitts, B. J. *Phys. Chem. Chem. Phys.* **2004**, *6*, 3879.
(41) Kleffmann, J.; Benter, T.; Wiesen, P. *J. Phys. Chem. A* **2004**, *108*, 5793.
(42) Mochida, M.; Finlayson-Pitts, B. J. *J. Phys. Chem. A* **2000**, *104*, 9705.
(43) Saliba, N.; Yang, H.; Finlayson-Pitts, B. J. *J. Phys. Chem. A* **2001**, *105*, 10339.
(44) Zhou, X.; Hi, Y.; Huang, G.; Thornberry, T. D.; Carroll, M. A.; Bertman, S. B. *Geophys. Res. Lett.* **2002**, *29*, DOI: 10.1029/2002GL015080.
(45) Zhou, X.; Civerolo, K.; Dai, H.; Huang, G.; Schwab, J.; Demerjian, K. *J. Geophys. Res.* **2002**, *107*, DOI: 10.1029/2001JD001539.
(46) Zhou, X. L.; Gao, H. L.; He, Y.; Huang, G.; Bertman, S. B.; Civerolo, K.; Schwab, J. *Geophys. Res. Lett.* **2003**, *30*, 2217.
(47) Ramazan, K. A.; Syomin, D.; Finlayson-Pitts, B. J. *Phys. Chem. Chem. Phys.* **2004**, *6*, 3836.
(48) Kleffmann, J.; Gavriloaiei, T.; Hofzumahaus, A.; Holland, F.; Koppmann, R.; Rupp, L.; Schlosser, E.; Siese, M.; Wahner, A. *Geophys. Res. Lett.* **2005**, *32*.
(49) Carter, W. P. L.; Atkinson, R.; Winer, A. M.; Pitts, J. N. J. *Int. J. Chem. Kinet.* **1981**, *13*, 735.
(50) Carter, W. P. L.; Atkinson, R.; Winer, A. M.; Pitts, J. N. J. *Int. J. Chem. Kinet.* **1982**, *14*, 1071.
(51) Carter, W. P. L.; Atkinson, R.; Winer, A. M.; Pitts, J. N. *Atmos. Environ.* **1985**, *19*, 1977.
(52) Sakamaki, F.; Akimoto, H. *Int. J. Chem. Kinet.* **1988**, *20*, 111.
(53) Killus, J. P.; Whitten, G. Z. *Int. J. Chem. Kinet.* **1990**, *22*, 547.
(54) Rohrer, F.; Bohn, B.; Brauers, T.; Brüning, D.; Johnen, F.-J.; Wahner, A.; Kleffman, J. *Atmos. Chem. Phys. Discuss.* **2004**, *4*, 7881.
(55) Sayer, R. M.; Horn, A. B. *Phys. Chem. Chem. Phys.* **2003**, *5*, 5229.
(56) White, J. U. *J. Opt. Soc. Am.* **1942**, *32*, 285.
(57) Calvert, J. G.; Pitts, J. N., Jr. *Photochemistry*; John Wiley and Sons: New York, 1966.
(58) Barney, W. S.; Wingen, L. M.; Lakin, M. J.; Brauers, T.; Stutz, J.; Finlayson-Pitts, B. J. *J. Phys. Chem. A* **2000**, *104*, 1692; *J. Phys. Chem. A* **2001**, *105*, 4166.
(59) McCurdy, P. R.; Hess, W. P.; Xantheas, S. S. *J. Phys. Chem. A* **2002**, *106*, 7628.
(60) Miller, Y.; Chaban, G. M.; Gerber, R. B. *Chem. Phys.* **2005**, *313*, 213.
(61) Dunning, T. H., Jr. *J. Chem. Phys.* **1989**, *90*, 1007.
(62) Kendall, R. A.; Dunning, T. H., Jr.; Harrison, R. J. *J. Chem. Phys.* **1992**, *96*, 6796.
(63) Chaban, G. M.; Jung, J. O.; Gerber, R. B. *J. Chem. Phys.* **1999**, *111*, 1823.
(64) Chaban, G. M.; Jung, J. O.; Gerber, R. B. *J. Phys. Chem. A* **2000**, *104*, 2772.
(65) Gerber, R. B.; Chaban, G. M.; Brauer, B.; Miller, Y. First Principles Calculations of Anharmonic Vibrational Spectroscopy of Large Molecules. In *Theory and Applications of Computational Chemistry: The First 40 Years*; Dykstra, C. E., Frenking, G., Kim, K. S., Scuseria, G. E., Eds.; Elsevier: Amsterdam, 2005; Chapter 9, p 165.
(66) Schmidt, M. W.; Baldridge, K. K.; Boatz, J. A.; Elbert, S. T.; Gordon, M. S.; Jensen, J. H.; Koseki, S.; Matsunaga, N.; Nguyen, K. A.; Su, S. J.; Windus, T. L.; Dupuis, M.; Montgomery, J. A. *J. Comput. Chem.* **1993**, *14*, 1347; http://www.msg.ameslab.gov/GAMESS/GAMESS.html.
(67) Harrick, N. J. *Internal Reflection Spectroscopy*; Interscience Publishers: New York, 1967.
(68) Foster, M. C.; Ewing, G. E. *J. Chem. Phys.* **2000**, *112*, 6817.
(69) Downing, H. D.; Williams, D. *J. Geophys. Res.* **1975**, *80*, 1656.
(70) Sumner, A. L.; Menke, E. J.; Dubowski, Y.; Newberg, J. T.; Penner, R. M.; Hemminger, J. C.; Wingen, L. M.; Brauers, T.; Finlayson-Pitts, B. J. *Phys. Chem. Chem. Phys.* **2004**, *6*, 604.
(71) Ritzhaupt, G.; Devlin, J. P. *J. Phys. Chem.* **1977**, *81*, 521.
(72) Sporleder, D.; Ewing, G. E. *J. Phys. Chem. A* **2001**, *105*, 1838.
(73) McGraw, G. E.; Bernitt, D. L.; Hisatsune, I. C. *J. Chem. Phys.* **1965**, *42*, 237.
(74) Guillory, W. A.; Bernstein, M. L. *J. Chem. Phys.* **1975**, *62*, 1058.
(75) Ritzhaupt, G.; Devlin, J. P. *J. Phys. Chem.* **1991**, *95*, 90.
(76) Smith, R. H.; Leu, M.-T.; Keiser, L. F. *J. Phys. Chem.* **1991**, *95*, 5924.
(77) Barnes, A. J.; Lasson, E.; Nielsen, C. J. *J. Mol. Struct.* **1994**, *322*, 165.
(78) Escribano, R.; Couceiro, M.; Gómez, P. C.; Carrasco, E.; Moreno, M. A.; Herrero, V. J. *J. Phys. Chem. A* **2003**, *107*, 651.
(79) Tao, F.-M.; Higgins, K.; Klemperer, W.; Nelson, D. D. *Geophys. Res. Lett.* **1996**, *23*, 1797.
(80) Staikova, M.; Donaldson, D. J. *Phys. Chem. Chem. Phys.* **2001**, *3*, 1999.
(81) Kjaergaard, H. G. *J. Phys. Chem. A* **2002**, *106*, 2979.
(82) Fernández, D.; Botella, V.; Herrero, V. J.; Escribano, R. *J. Phys. Chem.* **2003**, *107*, 10608.
(83) Dimitrova, Y. *Spectrochim. Acta A* **2004**, *60*, 1.
(84) Thompson, K. C.; Margey, P. *Phys. Chem. Chem. Phys.* **2003**, *5*, 2970.
(85) Thi, M. P.; Herzog-Cance, M. H.; Potier, A.; Potier, J. *J. Raman Spectrosc.* **1981**, *11*, 96.
(86) Kay, B. D.; Hermann, V.; Castleman, A. W. J. *Chem. Phys. Lett.* **1981**, *80*, 469.

(87) Zhang, X.; Mereand, E.; Castleman, A. W. J. *J. Phys. Chem.* **1994**, *98*, 3554.
(88) Gilligan, J. J.; Castleman, A. W. J. *J. Phys. Chem. A* **2001**, *105*, 5601.
(89) Davis, W. J.; DeBruin, H. J. *J. Inorg. Nucl. Chem.* **1964**, *26*, 1069.
(90) Tisdale, R. T.; Prenni, A. J.; Iraci, L. T.; Tolbert, M. A. *Geophys. Res. Lett.* **1999**, *26*, 707.
(91) Zundel, Z. In *The Hydrogen Bond, Recent Developments in Theory and Experiments*; Schuster, P., Zundel, Z., Sandorfy, C., Eds.; North-Holland: Amsterdam, 1976; Vol. 2, Chapter 15.
(92) Tolbert, M. A.; Middlebrook, A. M. *J. Geophys. Res.* **1990**, *95*, 22.
(93) Chen, W.-J.; Lo, W.-J.; Cheng, B.-M.; Lee, Y.-P. *J. Chem. Phys.* **1992**, *97*, 7167.
(94) Mack, J.; Bolton, J. R. *J. Photochem. Photobiol., A* **1999**, *128*, 1.
(95) Aschmann, S. M.; Atkinson, R. *J. Phys. Chem. A* **1997**, *101*, 8042.
(96) Syomin, D. A.; Finlayson-Pitts, B. J. *Phys. Chem. Chem. Phys.* **2003**, *5*, 5236.
(97) Sander, S. P.; Friedl, R. R.; Golden, D. M.; Kurylo, M. J.; Huie, R. E.; Orkin, V. L.; Moorgat, G. K.; Ravishankara, A. R.; Kolb, C. E.; Molina, M. J.; Finlayson-Pitts, B. J. *Chemical Kinetics and Photochemical Data for Use in Atmospheric Studies. Evaluation No. 14*; JPL Publ. No. 02-25; Jet Propulsion Laboratory: Pasadena, CA, 2002.
(98) Gauderman, W. J.; Avol, E.; Gilliland, F.; Vora, H.; Thomas, D.; Berhane, K.; McConnell, R.; Kuenzli, N.; Lurmann, F.; Rappaport, E.; Margolis, H.; Bates, D.; Peters, J. *New Engl. J. Med.* **2004**, *351*, 1057.
(99) Brown, E.; Gerber, R. B. Unpublished data, 2005.
(100) Prospero, J. M.; Nees, R. T. *Science* **1977**, *196*, 1196.
(101) Prospero, J. M.; Glaccum, R. A.; Nees, R. T. *Nature* **1981**, *289*, 570.
(102) Prospero, J. M.; Nees, R. T. *Nature* **1986**, *320*, 735.
(103) Prospero, J. M.; Schmitt, R.; Cuevas, E.; Savoie, D. L.; Graustein, W. C.; Turekian, K. K.; Volz-Thomas, A.; Diaz, A.; Oltmans, S. J.; Levy, H. *Geophys. Res. Lett.* **1995**, *22*, 2925.
(104) Prospero, J. M. *J. Geophys. Res.* **1999**, *104*, 15917.